

Recovery of Damaged Information and the Out-of-Time-Ordered Correlators

Bin Yan

*Center for Nonlinear Studies, Los Alamos National Laboratory, Los Alamos, New Mexico 87545 and
Theoretical Division, Los Alamos National Laboratory, Los Alamos, New Mexico 87545, USA*

Nikolai A. Sinitsyn

*Theoretical Division, Los Alamos National Laboratory, Los Alamos, New Mexico 87545, USA
(Dated: October 4, 2021)*

The evolution with a complex Hamiltonian generally leads to information scrambling. A time-reversed dynamics unwinds this scrambling and thus leads to the original information recovery. We show that if the scrambled information is, in addition, partially damaged by a local measurement, then such a damage can still be treated by application of the time-reversed protocol. This information recovery is described by the long-time saturation value of a certain out-of-time-ordered correlator of local variables. We also propose a simple test that distinguishes between quantum and reversible classical chaotic information scrambling.

In complex strongly correlated systems, local information spreads quickly over the whole system. This process is characterized by exponentially fast changes of the out-of-time ordered correlators (OTOCs) [1–4], such as the following correlator of local operators W and V with specific time ordering:

$$F(t) = \langle W^\dagger(t) V^\dagger(0) W(t) V(0) \rangle. \quad (1)$$

After OTOCs saturate, initially local information becomes encoded into global entanglement, hindering the data from local measurements.

It can be hard to recover this information if the scrambling path is not completely known or if the final state is partly damaged. For instance, a single qubit thrown into a black hole is quickly dispersed and lost behind the horizon. With the resource of early Hawking radiation, only a few qubits of information emitted from the black hole are needed to reconstruct the lost qubit [5] but there is no simple recipe for how to do this without considerable knowledge about the system [6–8].

In order to suggest a solution to similar problems, we consider a practically accessible scenario for information scrambling and unscrambling. Let us describe this scenario as a hypothetical application of a quantum processor, such as the one in the quantum supremacy test [9], for hiding quantum information. Our processor can be simpler than that in Ref. [9] because we require that only one of the qubits can be prepared and measured, which is suitable for experiments with liquid-NMR quantum computers [10, 11].

Let Alice have such a processor that implements fast information scrambling during a reversible unitary evolution of many interacting qubits. She applies this evolution to hide an original state of one of her qubits, which we call the central qubit. The other qubits are called the bath. To recover the initial central qubit state, Alice can apply a time-reversed protocol.

Let Bob be an intruder who can measure the state of the central qubit in any basis unknown to Alice, as shown in Fig. 1. If her processor has already scrambled the information, Alice is sure that Bob cannot get anything

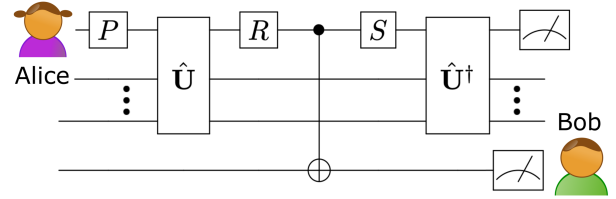


FIG. 1. The protocol: Alice prepares the central qubit with the gate P , and applies the scrambling unitary \hat{U} . Bob measures the central qubit in any basis defined by the gate R , with S flipping the qubit to the corresponding post measurement state. Alice is still able to reconstruct the encoded information via a single decoding unitary \hat{U}^\dagger .

useful. However, Bob's measurement changes the state of the central qubit and also destroys all quantum correlations between this qubit and the rest of the system. According to the no-hiding theorem [12], information of the central qubit is completely transferred to the bath during the scrambling process. However, Alice does not have knowledge of the bath state at any time. How can she recover the useful information in this case?

In this Letter, we show that even after Bob's measurement, Alice can recover her information by applying the time-reversed protocol and performing a quantum state tomography with a limited amount of effort. Moreover, reconstruction of the original qubit will not be influenced by Bob's choice of the measurement axis and the initial state of the bath.

This effect cannot be explained with semiclassical intuition. Indeed, classical chaotic evolution magnifies any state damage exponentially quickly, which is known as the butterfly effect. The quantum evolution, however, is linear. This explains why, in our case, the uncontrolled damage to the state is not magnified by the subsequent complex evolution. Moreover, the fact that Bob's measurement does not damage the useful information follows from the property of entanglement correlations in the scrambled state [12]. Hence, the information recovery effect can be used in practice to distinguish quan-

tum scrambling from the scrambling achieved via classical chaotic dynamics.

Suppose that the process in Fig. 1 is realized in a system of qubits (spins-1/2's). The system starts from an initial product state, $\rho_0 = |i\rangle\langle i| \otimes \rho_B$. Here, the central qubit state $|i\rangle$ encodes the information to be scrambled and recovered, whereas ρ_B of the bath qubits can be an arbitrary pure or mixed state.

After a unitary evolution during time t_1 , a projective measurement along a random axis is applied to the central spin, without collecting any data from the measurement outcome. Then, the system evolves backward in time during t_2 , followed by a state tomography for the central spin. We claim that when $t_2 = t_1$, the final measurements contain information that can be used to fully reconstruct the initial state of the central qubit.

Two remarks are in order. First, the recovery of damaged information is a generic effect insensitive to the detailed dynamics, as long as the unitary evolution is complex enough to scramble the information. Thus, for any initial state, after the scrambling process the reduced density matrix of the central qubit becomes maximally mixed. For instance, the desired scrambling unitary can be generated by a chaotic many-body Hamiltonian, or be comprised by random two-qubit unitaries on a quantum circuit. Second, the initial information is fully recovered at the moment $t_2 = t_1$, i.e., right after the backward unitary becomes conjugated to the forward unitary, but it will be useful to explore what happens for $t_2 \neq t_1$.

Let \hat{P}_r be the projection operator for Bob's measurement on the central qubit. There are two complementary histories in which, after Bob's measurement, the central spin state is projected to the subspace described by either \hat{P}_r or $\hat{\mathbb{I}} - \hat{P}_r$. The probability for Alice's projective measurement \hat{P}_f at the final time moment is

$$\text{Prob}(\hat{P}_f) = \int [dr] \text{Prob}(\hat{P}_f, \hat{P}_r) + \text{Prob}(\hat{P}_f, \hat{\mathbb{I}} - \hat{P}_r), \quad (2)$$

where $\text{Prob}(\hat{P}_f, \hat{P}_r)$ is the joint probability that both Alice and Bob find unit measurement outcomes for their measurement operators. Note that, since we do not collect results of the Bob's intermediate measurements, his complementary measurement outcome contributes to $\text{Prob}(\hat{P}_f)$ as well. The integral over r in Eq. (2) accounts for averaging over an arbitrary distribution of possible directions for Bob's measurement axes.

Let $\hat{U}(t_1)$ be the evolution operator for the time-forward protocol during time t_1 and $\hat{U}^\dagger(t_2)$ be the evolution operator for the time-reversed protocol during time t_2 . The probability of the nonzero outcome for the intermediate measurement \hat{P}_r and the corresponding post measurement state ρ_r are then given by

$$\begin{aligned} \text{Prob}(\hat{P}_r) &= \text{tr} \hat{P}_r \rho(t_1) \hat{P}_r, \\ \rho_r &= \hat{P}_r \rho(t_1) \hat{P}_r / \text{Prob}(\hat{P}_r), \end{aligned} \quad (3)$$

where $\rho(t_1) = \hat{U}(t_1) \rho_0 \hat{U}^\dagger(t_1)$ is the system state at time t_1 . The probability for the final measurement \hat{P}_f , con-

ditioned on the system being projected to the post measurement state ρ_r , is

$$\text{Prob}(\hat{P}_f | \hat{P}_r) = \text{tr} \left(\hat{P}_f \hat{U}(t_2) \rho_r \hat{U}^\dagger(t_2) \hat{P}_f \right). \quad (4)$$

This gives the desired joint probability $\text{Prob}(\hat{P}_f, \hat{P}_r) = \text{Prob}(\hat{P}_f | \hat{P}_r) \text{Prob}(\hat{P}_r)$. Since the system is initially in the state $\rho_0 = |i\rangle\langle i| \otimes \rho_B$, the joint probability can be expressed in a compact form:

$$\text{Prob}(\hat{P}_f, \hat{P}_r) = \langle \hat{P}_r(t_1) \hat{P}_f(t_1 - t_2) \hat{P}_r(t_1) \hat{P}_i \rangle. \quad (5)$$

Here, the ensemble average is defined as $\langle \bullet \rangle \equiv \text{tr}(\bullet \hat{\mathbb{I}} \otimes \rho_B)$. Equation (5) shows that the effect of Bob's interference on the information that Alice obtains after applying the time-reversed protocol is described by a two-time OTOC of projection operators.

Let us now express this OTOC (5) in terms of Pauli operators, using the identity $\hat{\sigma}_\phi \equiv 2\hat{P}_\phi - \hat{\mathbb{I}}$. We are interested in long scrambling times and $t_2 \sim t_1$. The second order spin correlators, such as $\langle \hat{\sigma}_f(t_1) \hat{\sigma}_i \rangle$, decay quickly with time. Hence, we can safely neglect all such correlators except the ones that depend on $t_1 - t_2 \ll t_1$. The joint probability is then

$$\begin{aligned} \text{Prob}(\hat{P}_f, \hat{P}_r) &= \frac{1}{4} + \frac{1}{16} \langle \hat{\sigma}_f(t_1 - t_2) \hat{\sigma}_i \rangle + \\ &+ \frac{1}{16} \langle \hat{\sigma}_r(t_1) \hat{\sigma}_f(t_1 - t_2) \hat{\sigma}_r(t_1) \hat{\sigma}_i \rangle. \end{aligned} \quad (6)$$

For $t_1 = t_2$, the second term on the right-hand side in Eq. (6) is independent of the evolution unitary. All such details are hidden in the third term. At $t_1 = t_2$, this four-point correlator becomes a standard spin OTOC, i.e.,

$$F(t) = \langle \hat{\sigma}_r(t) \hat{\sigma}_i \hat{\sigma}_r(t) \hat{\sigma}_f \rangle. \quad (7)$$

For finite t and for a small bath this correlator has a non-trivial system-specific behavior that obscures the contribution of $\langle \hat{\sigma}_f(t_1 - t_2) \hat{\sigma}_i \rangle$ in Eq. (6). However, we are interested in the typical complex unitary evolution that scrambles information. Hence, we claim that $F(t)$ saturates to a universal value that is described by its average over an ensemble of random unitaries. This average can be evaluated as an integral over all unitaries with respect to the Haar measure [13, 14], i.e.,

$$\bar{F} = \int_{\text{Haar}} dU \text{tr} [U^\dagger \sigma_r U \sigma_i U^\dagger \sigma_r U \sigma_f \rho_B], \quad (8)$$

where ρ_B is the initial state of bath qubits. The integral can be further calculated using the identity for Haar unitaries [7]:

$$\begin{aligned} &\overline{U_{m_1 n_1} U_{m'_1 n'_1}^* U_{m_2 n_2} U_{m'_2 n'_2}^*} \\ &= \frac{\delta_{m_1 m'_1} \delta_{m_2 m'_2} \delta_{n_1 n'_1} \delta_{n_2 n'_2} + \delta_{m_1 m'_2} \delta_{m_2 m'_1} \delta_{n_1 n'_2} \delta_{n_2 n'_1}}{N^2 - 1} \\ &- \frac{\delta_{m_1 m'_1} \delta_{m_2 m'_2} \delta_{n_1 n'_2} \delta_{n_2 n'_1} + \delta_{m_1 m'_2} \delta_{m_2 m'_1} \delta_{n_1 n'_1} \delta_{n_2 n'_2}}{N(N^2 - 1)}, \end{aligned} \quad (9)$$

where N is the dimension of the Hilbert space. After summing over all indices and using a trivial identity $\text{tr}(\hat{\sigma}_{f,i,r}) = 0$, the average reduces to

$$\bar{F} = \langle \sigma_i \sigma_f \rangle / (N^2 - 1) \equiv \text{tr}(\sigma_i \sigma_f \otimes \rho_B) / (N^2 - 1). \quad (10)$$

We need this formula only for $N \gg 1$ because then a single typical unitary produces the effect that coincides with the average of the OTOC. The large denominator, for $N \rightarrow \infty$, makes this OTOC decay to zero. Since this happens for random unitary evolution, the same is true for sufficiently long scrambling times and sufficiently large baths, so the fourth order correlator in Eq. (6) also vanishes.

After averaging over random unitaries, the joint probability $\text{Prob}(\hat{P}_f, \hat{P}_r)$ is the same as $\text{Prob}(\hat{P}_f, \hat{\mathbb{I}} - \hat{P}_r)$, so the final probability is twice that of $\text{Prob}(\hat{P}_f, \hat{P}_r)$ for any distribution of Bob's measurement axes. Equation (6) reduces then to

$$\text{Prob}(\hat{P}_f) = \frac{1}{2} + \frac{1}{8} \langle \hat{\sigma}_f(t_1 - t_2) \hat{\sigma}_i \rangle. \quad (11)$$

This is the main result of our work. It shows that Alice's measurement probability at $t_2 = t_1$ can be used to construct the initial state of the central qubit, i.e., $\rho_i = (\hat{\mathbb{I}} + \hat{\sigma}_i)/2$. This information returns to the central qubit during a short central spin lifetime, as it is described by a second order spin correlator. The state of the central qubit at $t_2 = t_1$ is

$$\rho_f(t_2 = t_1) = \frac{1}{4} \hat{\mathbb{I}} + \frac{1}{2} \rho_i. \quad (12)$$

Note that the central qubit ends up in a partially mixed state. However, distinct initial states are transformed to distinct final states, i.e., the map is injective. Hence, the initial state can be extracted from the final state statistically, using quantum state tomography. Importantly, this can be done with any precision using only a finite ensemble of our system because the coherent contribution in Eq. (12) is not suppressed by the complexity of the unitary evolution.

The model of a nuclear spin bath.— Our discussion of information recovery is applicable to all systems that show quantum information scrambling [15]. Thus, this effect should be possible to demonstrate with a processor that was used in the quantum supremacy test [9], as well as in simulations of the SYK model [2, 16] driven according to the protocol in Fig. 1.

As an example of that the Haar random unitary provides a correct description of the behavior of OTOCs, we studied numerically the nuclear spin-bath model. This model has been frequently used to describe interactions of a solid state qubit with nuclear spins [17, 18]. Its Hamiltonian is

$$H = \sum_{i=1}^{N_s} \sum_{\alpha} J_i^{\alpha} S^{\alpha} s_i^{\alpha}, \quad \alpha = x, y, z, \quad (13)$$

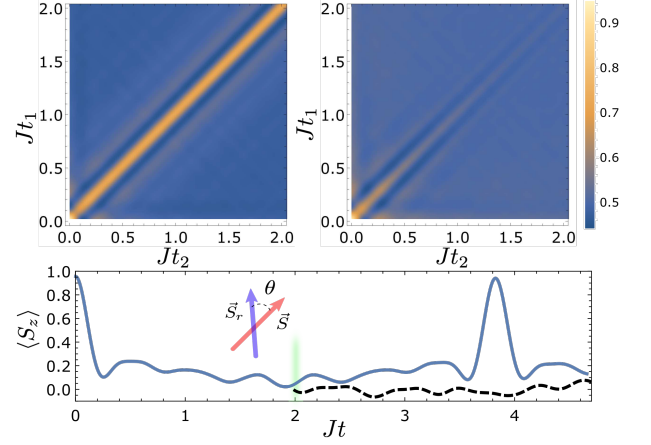


FIG. 2. Top: Final measurement probabilities obtained from numerical simulations of the model (13) with quantum spins. Left and right panels correspond to the final probabilities deduced from the joint probability (5) and (14), respectively. Bottom: Dynamics of the z component of the central spin vector in model (13) with all classical spins. The green bar marks time t_1 with invasive measurement of the central spin. Black dashed curve and blue solid curve correspond to the cases with and without intermediate invasive measurement, respectively. $N_s = 10$ and $N_s = 30$ for quantum and classical simulations, respectively.

where the couplings J_i^{α} are independent Gaussian distributed random numbers with zero mean and standard deviation J . Here, the central spin-1/2, S , interacts with the bath of N_s spins-1/2's, s_i . We simulated the Schrödinger equation with this Hamiltonian numerically to obtain the effect of the unitary evolution.

In our simulations, the central spin starts from the $|\uparrow\rangle$ state, i.e., $\sigma_i = \sigma_z$ in Eq. (11). The bath spins are prepared in a maximally mixed state. This corresponds to a common situation of practically infinite temperature for nuclear spins. Figure 2 (top left) shows the obtained final Alice's probability of a nonzero measurement result for $\sigma_f = \sigma_z$ and a fixed randomly chosen σ_r . It does show the echo effect along the $t_1 = t_2$ line, in perfect quantitative agreement with Eq. (11). No additional averaging over Bob's measurement axes and parameters J_i^{α} is needed for a quantitative agreement with Eq. (11). We also verified numerically for $N_s = 10$ (not shown) that the same universal result is obtained for several other choices of the initial density matrix of the spin bath.

It is instructive to compare the echo in OTOC with another type of spin echo, which is induced by a similar protocol, in which the backward evolution $\hat{U}^{\dagger}(t_2)$ is replaced by the forward one $\hat{U}(t_2)$. The joint probability is then described by the correlator (5) with t_2 replaced by $-t_2$, i.e.,

$$\text{Prob}_2(\hat{P}_f, \hat{P}_r) = \langle \hat{P}_r(t_1) \hat{P}_f(t_1 + t_2) \hat{P}_r(t_1) \hat{P}_i \rangle. \quad (14)$$

This correlator can be measured in solid state systems by standard means, for example, it was studied experimentally in semiconductor quantum dots [19] (see also

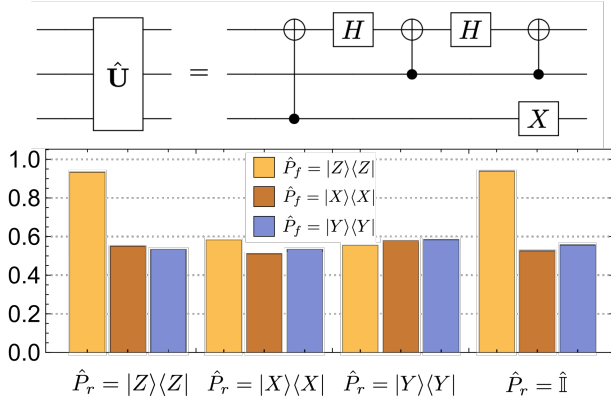


FIG. 3. Top: The realization of the unitary (15). Bottom: Statistics of the measurement probabilities obtained with the IBM-Q processor. Colors label orthogonal final measurements of \hat{P}_f . The three groups of the chart correspond to orthogonal intermediate measurements \hat{P}_r . The basis is $|Z\rangle = |0\rangle$, $|X\rangle = (|0\rangle + |1\rangle)/\sqrt{2}$, and $|Y\rangle = (|0\rangle + i|1\rangle)/\sqrt{2}$. The final measurement probabilities, after averaging over intermediate outcomes, read as 0.5426, 0.5522, and 0.7529, for $\hat{P}_f = |X\rangle\langle X|$, $|Y\rangle\langle Y|$, and $|Z\rangle\langle Z|$, respectively.

Ref. [20]). As we show in Fig. 2 (top right), the final probability (14) also shows an echo effect near $t_2 = t_1$. However, this echo originates from a finite scrambling rate and therefore decays at large times, in sharp contrast to the echo in the OTOC.

Quantum vs classical scrambling.— Our observation can be used to additionally validate quantum supremacy tests such as in Ref. [9]. There is only a finite depth for precise simulations of classical chaotic motion with classical digital computers because of the exponential increase of round-off errors [21]. Therefore, a classical analog computer with nonlinear interactions between its components can evolve reversibly to a state that cannot be predicted with classical digital computers. Hence, to validate quantum supremacy, an additional test may be needed to prove that we deal with a quantum scrambled state at the end rather than with a state generated by classical chaos [22].

In the classical case, a small change of the state vector at the end of the forward protocol would be quickly magnified during the backward time evolution. Thus, the state at the end of our control protocol would be strongly different from the initial one.

To illustrate this, we simulated the evolution of interacting classical spins with the same Hamiltonian (13) subject to the classical Landau-Lifshitz equations [23]. The state of a classical spin is specified by a three dimensional unit vector. Our initial state for the central spin is a unit vector pointing along the z axis. Bath spins start from random directions. Instead of quantum projective measurements, we assumed that classical measurements were invasive. Namely, a measurement resets the classical spin to be directed either along or opposite to the measurement axis with probabilities $\cos^2(\theta/2)$ or

$1 - \cos^2(\theta/2)$, respectively, where $\theta \in [0, \pi]$ is the angle between the central spin vector and the direction of the measurement axis. The time-reversed dynamics was induced by changing the sign of all spin coupling constants.

Figure 2 (bottom) shows the evolution of the z component of the central classical spin during the time of the protocol. As expected, an intermediate invasive measurement of only the central spin has lead then to a state with unrecoverable initial information, in sharp contrast to the quantum case.

IBM-Q experiment.— To verify that our predictions are robust against weak natural decoherence that is always present in modern quantum computers, we performed an experiment with the IBM-Q five-qubit processor. The main programmed system consisted of one central and two bath qubits. We also added an ancillary qubit to effectively realize measurement by entanglement of this and the central qubit.

The quantum circuit is the same as in Fig. 1. Here, the three qubit unitary is given by

$$\hat{U} = \mathbb{I} \otimes |01\rangle\langle 00| + \sigma_x \otimes |00\rangle\langle 01| - i\sigma_y \otimes |11\rangle\langle 10| - \sigma_z \otimes |10\rangle\langle 11|, \quad (15)$$

with the corresponding quantum circuit realization shown in Fig. 3 (top) [24]. It maps any initial state $|i\rangle$ of the target qubit to the maximally mixed state, provided that the input states of the bath qubits are $|+\rangle = (|0\rangle + |1\rangle)/\sqrt{2}$. This unitary is not a typical Haar random unitary, since its scrambling effect depends on the bath's initial state. Consequently, the four point correlator at $t_2 = t_1$ in Eq. (6), i.e., $\langle \hat{U} \hat{\sigma}_r \hat{U}^\dagger \hat{\sigma}_f \hat{U} \hat{\sigma}_r \hat{U}^\dagger \hat{\sigma}_i \rangle$, is not zero, even after averaging $\hat{\sigma}_r$ over random Pauli matrices (corresponding to random intermediate projective measurements). Instead, it makes the above four point correlator vanish when $\hat{\sigma}_r$ is averaged over the Pauli group. Thus, if we include the identity operator as part of the intermediate measurement, the rest of the protocol and the final result will not change.

The central qubit starts at $|0\rangle$. We perform the final measurements along three orthogonal directions, corresponding to $|0\rangle$, $(|0\rangle + |1\rangle)/\sqrt{2}$, and $(|0\rangle + i|1\rangle)/\sqrt{2}$. The theoretical probabilities for these final measurements are 0.75, 0.5, and 0.5, respectively. Figure 3 shows the statistics of the final measurements, obtained with the IBM 5-qubit processor, from which we inferred the initial state $0.992|0\rangle - (0.082 - 0.101i)|1\rangle$. This corresponds to 0.983 fidelity, which means that natural decoherence was not detrimental.

The effect of damaged information recovery should be accessible for verification in more complex systems using capabilities in the generation of random unitary evolution [9–11]. In addition, we showed that this effect is described by the long-time saturation values of OTOCs. This observation reveals a novel domain of applications for such unusual correlators.

This effect becomes very counterintuitive if we interpret unitaries U and U^\dagger in Fig. 1 as, respectively, back-

ward and forward time travel operators. Then, the intermediate Bob’s measurement is expected to lead to the same butterfly effect as the one in the famous Ray Bradbury’s story “A Sound of Thunder” [25]. In that story, a character used a time machine to travel to the deep past, stepped on an insect there, and after returning to the present time found a totally different world. In contrast, our result shows that by the end of a similar protocol the local information is essentially restored.

ACKNOWLEDGMENTS

We would like to thank Avadh Saxena and Wojciech Zurek for comments and suggestions. This work was supported by the U.S. Department of Energy, Office of Science, Basic Energy Sciences, Materials Sciences and Engineering Division, Condensed Matter Theory Program.

-
- [1] A. Larkin and Y. N. Ovchinnikov, *Sov. Phys. JETP* **28**, 1200 (1969).
 - [2] A. Kitaev, A simple model of quantum holography, in *Proceedings of the KITP Program: Entanglement in Strongly-Correlated Quantum Matter*, 2015 (Kavli Institute for Theoretical Physics, Santa Barbara, 2015), Vol. 7.
 - [3] Juan Maldacena, Stephen H Shenker, and Douglas Stanford, “A bound on chaos,” *Journal of High Energy Physics* **2016**, 106 (2016).
 - [4] Brian Swingle, “Unscrambling the physics of out-of-time-order correlators,” *Nature physics* **14**, 988–990 (2018).
 - [5] Patrick Hayden and John Preskill, “Black holes as mirrors: quantum information in random subsystems,” *Journal of High Energy Physics* **2007**, 120 (2007).
 - [6] K A Landsman, C Figgatt, T Schuster, N M Linke, B Yoshida, N Y Yao, and C Monroe, “Verified quantum information scrambling,” *Nature* **567**, 61–65 (2019).
 - [7] B Vermersch, A Elben, L M Sieberer, N Y Yao, and P Zoller, “Probing scrambling using statistical correlations between randomized measurements,” *Physical Review X* **9**, 021061 (2019).
 - [8] Beni Yoshida and Norman Y Yao, “Disentangling scrambling and decoherence via quantum teleportation,” *Physical Review X* **9**, 011006 (2019).
 - [9] Frank Arute *et al.*, “Quantum supremacy using a programmable superconducting processor,” *Nature* **574**, 505–510 (2019).
 - [10] Jun Li, Ruihua Fan, Hengyan Wang, Bingtian Ye, Bei Zeng, Hui Zhai, Xinhua Peng, and Jiangfeng Du, “Measuring Out-of-Time-Order correlators on a nuclear magnetic resonance quantum simulator,” *Physical Review X* **7**, 031011 (2017).
 - [11] Jharana Rani Samal, Arun K Pati, and Anil Kumar, “Experimental test of the quantum no-hiding theorem,” *Physical Review Letters* **106**, 080401 (2011).
 - [12] Samuel L Braunstein and Arun K Pati, “Quantum information cannot be completely hidden in correlations: implications for the black-hole information paradox,” *Physical Review Letters* **98**, 080502 (2007).
 - [13] J. Cotler, N. Hunter-Jones, J. Liu, and B. Yoshida, “Chaos, complexity, and random matrices,” *J. High Energy Phys.* **2017**, 48 (2017).
 - [14] Bin Yan, Lukasz Cincio, and Wojciech H Zurek, “Information scrambling and loschmidt echo,” *Physical Review Letters* **124**, 160603 (2020).
 - [15] Supplementary Material provides an additional numerical proof of our predictions for the scrambling unitaries that were constructed as quantum circuits made of randomly generated two-qubit unitary gates.
 - [16] S. Sachdev and J. Ye, “Gapless spin-fluid ground state in a random quantum Heisenberg magnet,” *Phys. Rev. Lett.* **70**, 3339–3342 (1993).
 - [17] Nina Fröhling and Frithjof B Anders, “Long-time coherence in fourth-order spin correlation functions,” *Physical Review B* **96**, 045441 (2017).
 - [18] Nina Fröhling, Frithjof B Anders, and Mikhail Glazov, “Nuclear spin noise in the central spin model,” *Physical Review B* **97**, 195311 (2018).
 - [19] A Bechtold, F Li, K Müller, T Simmet, P-L Ardel, J J Finley, and N A Sinitsyn, “Quantum effects in Higher-Order correlators of a Quantum-Dot spin qubit,” *Physical Review Letters* **117**, 027402 (2016).
 - [20] R-B Liu, S-H Fung, H-K Fung, A N Korotkov, and L J Sham, “Dynamics revealed by correlations of time-distributed weak measurements of a single spin,” *New Journal of Physics* **12**, 013018 (2010).
 - [21] Pengliang Shi, “A relation on round-off error, attractor size and its dynamics in driven or coupled logistic map system,” *Chaos* **18**, 013122 (2008).
 - [22] Robert Alicki, “On the meaning of “quantum supremacy” experiments,” (2020), [arXiv:2001.00791](https://arxiv.org/abs/2001.00791) [quant-ph].
 - [23] N A Sinitsyn, Yan Li, S A Crooker, A Saxena, and D L Smith, “Role of nuclear quadrupole coupling on decoherence and relaxation of central spins in quantum dots,” *Physical review letters* **109**, 166605 (2012).
 - [24] This unitary was used before to demonstrate the no-hiding theorem on the quantum computers [26].
 - [25] Ray Bradbury, “A sound of thunder,” *Collier’s Weekly* June 28 (1952).
 - [26] Amolak Ratan Kalra, Navya Gupta, Bikash K Behera, Shiroman Prakash, and Prasanta K Panigrahi, “Demonstration of the no-hiding theorem on the 5-qubit IBM quantum computer in a category-theoretic framework,” *Quantum Information Processing* **18**, 170 (2019).

Supplementary Material for
“Recovery of Damaged Information and the Out-of-Time Order Correlators”

Appendix A: Random Circuit Model

Here, we show the results of our numerical study of information scrambling in a quantum circuit model composed of random two-qubit gates. This provides a different, from the nuclear spin model, illustration of the information recovery effect, at conditions that mimic computations by the Google’s processor for testing quantum supremacy. We also explore here the deviations from our theoretical predictions due to the finite system size effects.

The probability for the final measurement \hat{P}_f (at $t_2 = t_1$), after averaging over random scrambling unitaries, was shown (Eqs. (10) and (11) in the main text) to be

$$\text{Prob}(\hat{P}_f) = \frac{1}{2} + \frac{1}{8} \langle \hat{\sigma}_f \hat{\sigma}_i \rangle + \bar{F}, \quad (\text{A1})$$

where the term \bar{F} is the Haar average of an OTOC, i.e.,

$$\bar{F} = \int_{\text{Haar}} dU \text{tr} [U^\dagger \sigma_r U \sigma_i U^\dagger \sigma_r U \sigma_f \rho_B] = \text{tr}(\sigma_i \sigma_f \otimes \rho_B) / (N^2 - 1), \quad (\text{A2})$$

where N is the dimension of the Hilbert space. Hence, \bar{F} vanishes rapidly with increasing system size.

We claim that for relatively large system size a single typical scrambling unitary is representative, i.e., it gives a result that agrees with \bar{F} up to negligible finite size fluctuations. Generally, it is sufficient to show for a large number of qubits that the deviation between the typical OTOC value and \bar{F} is vanishing. This deviation is characterized by

$$C = \int_{\text{Haar}} dU \left([\text{Prob}_U(\hat{P}_f)]^2 - [\text{Prob}(\hat{P}_f)]^2 \right). \quad (\text{A3})$$

Here $\text{Prob}_U(\hat{P}_f)$ is the measurement probability for a single scrambling unitary U . We expect that fluctuations decrease with the system size as,

$$C \sim N^{-1}, \quad (\text{A4})$$

where N is the size of the phase space $N = 2^{n_q}$, and where n_q is the number of qubits.

To test this prediction, we simulated numerically the dynamics induced by a quantum circuit composed of random two-qubit unitaries. Namely, the global random scrambling unitary in the protocol is composed of random two-qubit unitaries, as illustrated in Fig. A1 of this supplementary. In our simulations, each scrambling unitary was generated with 1000 layers of such two qubit unitaries. All input states of the qubits were prepared in computational $|0\rangle$.

Figure A2 shows the final numerically obtained measurement probabilities, $\text{Prob}(\hat{P}_f)$ for different single runs of the protocol in Fig. 1 of the main text for eight qubits. The results show very small fluctuations, for each randomly chosen unitary, around the theoretically predicted mean values.

By measuring such deviations for different numbers of qubits, we studied the fluctuation scaling with the increasing system size. Fig. A3 shows the numerically extracted fluctuations for different numbers of qubits in the system. The scaling is well described by $\sim N^{-1}$.

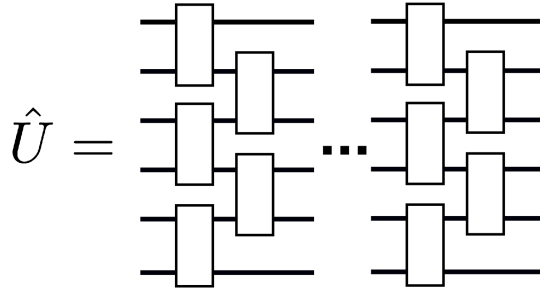


FIG. A1. The global scrambling unitary is composed of multiple layers of random two-qubit gates. Each two-qubit gate is drawn from the unitary group with respect to Haar measure.

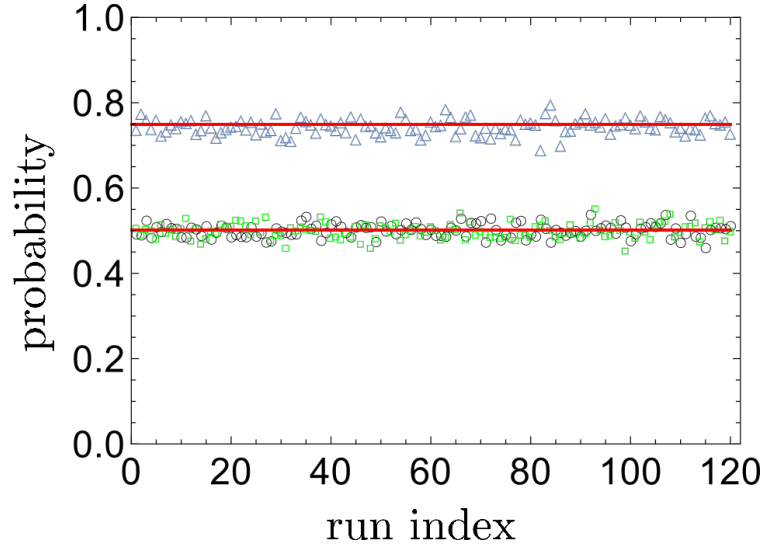


FIG. A2. Final Alice's measurement probabilities for many individual runs, with different random unitary evolution. Blue triangles, green squares, and black circles correspond to final projective measurements $|Z\rangle\langle Z|$, $|X\rangle\langle X|$, and $|Y\rangle\langle Y|$, respectively, where $|X\rangle = |0\rangle$, $|Y\rangle = (|0\rangle + |1\rangle)/\sqrt{2}$, and $(|0\rangle + i|1\rangle)/\sqrt{2}$. Red and orange lines are the theoretically predicted values.

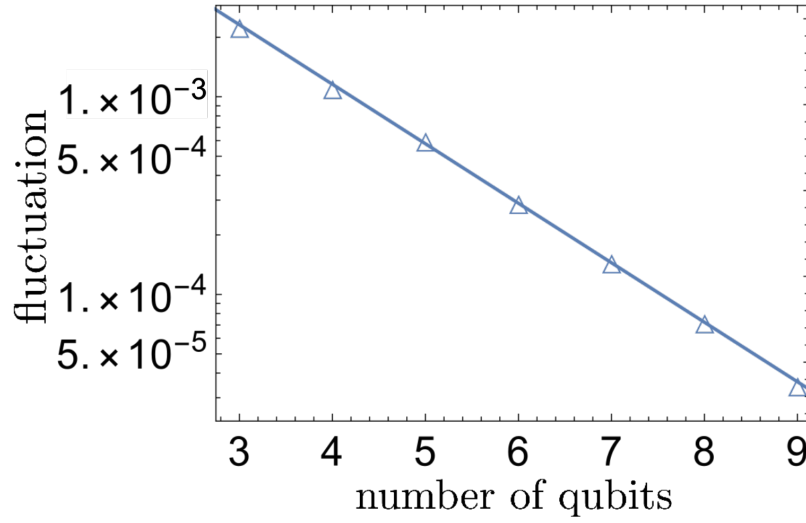


FIG. A3. Fluctuation variance (A3) for different numbers of qubits. Triangles correspond to numerically obtained values for the variance. The solid curve is the fit by the $\sim e^{-n_q}$ curve, where n_q is the number of qubits. This proves that deviations from our theoretical predictions are suppressed with the number of qubits exponentially quickly.